Buckling of a linear chain of hard spheres in a harmonic confining potential

Hutzler, Stefan; Mughal, Adil; Ryan-Purcell, John; Irannezhad, Ali; Weaire, Denis

Published in:
Physical Review E

DOI:
10.1103/PhysRevE.102.022905

Publication date:
2020

Citation for published version (APA):
Hutzler, S., Mughal, A., Ryan-Purcell, J., Irannezhad, A., & Weaire, D. (2020). Buckling of a linear chain of hard spheres in a harmonic confining potential: Numerical and analytical results for low and high compression. *Physical Review E*, *102*(2), [022905]. https://doi.org/10.1103/PhysRevE.102.022905

Buckling of a linear chain of hard spheres in a harmonic confining potential: numerical and analytical results for low and high compression

Stefan Hutzler,[1,*] Adil Mughal,[2] John Ryan-Purcell,[1] Ali Irannezhad,[1] and Denis Weaire[1]

[1] *School of Physics, Trinity College Dublin, Dublin 2, Ireland*

[2] *Department of Mathematics, Aberystwyth University, Penglais, Aberystwyth, Ceredigion, Wales SY23, United Kingdom*

(Dated: July 22, 2020)

Abstract

We extend a previous analysis of the buckling properties of a linear chain of hard spheres between hard walls under transverse harmonic confinement. Two regimes are distinguished - low compression, for which the entire chain buckles, and higher compression, for which there is localised buckling. With further increase of compression, second-neighbour contacts occur; beyond this compression the structure is no longer planar, and is not treated here. A continuous model is developed which is amenable to analytical solution in the low compression regime for an infinite chain. This is helpful in understanding the scaling properties of both finite and infinite chains.

* permanent address: School of Physics, Trinity College Dublin, Dublin 2, Ireland; stefan.hutzler@tcd.ie

I. INTRODUCTION

In this paper we examine an elementary problem: the buckling of a linear chain of hard spheres. The spheres are confined between opposing hard walls while also being confined in the transverse direction by a harmonic potential. The linear chain is unstable under the slightest compression and forms a range of buckled zigzag structures with increasing compression. Below a critical compression the structure remains planar so we may instead speak of *disks* in two dimensions. At higher compressions, more complex three-dimensional structures emerge. **A description in terms of disks is natural for the theory, but we will use the term "spheres" throughout, as a reminder of the nature of the relevant experiments.**

Our work bears many similarities to studies of the jamming of disks in a narrow channel [1], [2] and [3], an extension to the jamming of disks in a centrifuge, similar to the confining harmonic potential presented in this paper, was carried out in [4]. However, the approach in these studies is usually a statistical one, using methods such as Monte Carlo simulations [5] to find jammed structures. Our method relies on a recursion relation. This has the advantage of being simple and amenable to both numerical and analytical treatment.

Despite its simplicity such a model can stand as a tractable prototype for a more general class of physical systems that include soft particles and/or long-range interactions. We expect this work to find applications in a range of experiments involving zigzagging linear chains of particles. Examples include cold ions in traps [6–12], dusty plasmas [13], droplets in microfluidic crystals [14], paramagnetic colloidal particles in an external field [15] and linear chains of magnetic spheres [16, 17].

Following up on a preliminary investigation of the initial stage of buckling [18], here we will analyse it more exhaustively and adduce a new *continuous* model for

low-compression properties of the discrete chain.

We will examine two kinds of bifurcation diagrams that represent the proliferation of alternative equilibria (both stable and unstable) at higher compression. The first of these diagrams deals with relative energy and is an improved version of that previously reported [18]. The second represents the position at which buckling is localised for each of the alternative equilibrium states. If each branch of such a bifurcation diagram is pursued to higher compressions it terminates, in the sense that second-nearest neighbours come into contact; the structure becomes non-planar, and the methods used here are inadequate. Anything beyond this is therefore reserved for further studies, as is the exploration of buckling properties of soft spheres and the determination of Peierls-Nabarro potentials.

Fig. 1 shows an illustrative example from an elementary experiment, described in detail in section VIII.

In the following we begin by describing the model and the numerical scheme that we use, after which we present detailed results from simulations for the buckling of a linear chain of $N = 5, 6, 7$ and 8 hard spheres. In the limit of low compressions we adduce analytical results, based on a continuous approximation, which are compared with simulations. Finally, we present exemplary experiments which are directly compared with simulations.

II. UNIFORM ZIGZAG

Before giving the details of our methods we describe the closely related case of the *uniform zigzag* arrangement of hard spheres, which is the equilibrium arrangement if periodic boundary conditions are applied to a finite chain (with an even number of spheres), as shown in Fig 2. The analysis of the uniform zigzag is very elementary. All of the structures discussed below are modulated versions of it, conforming to

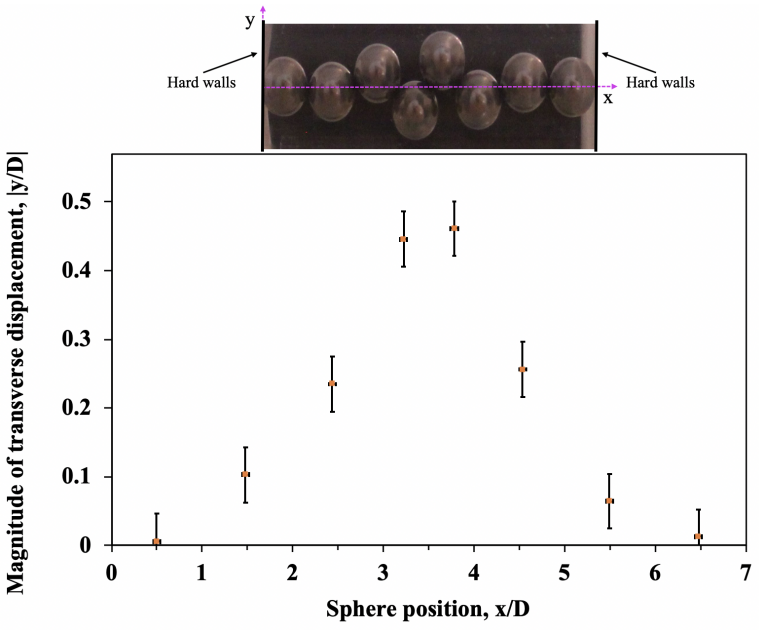

FIG. 1: Photograph of an elementary experiment (described in Section VIII) showing a chain of $N = 8$ hard spheres under compression. Also shown are the magnitudes of the transverse displacements of the sphere centres. Both the values for position and displacement relative to the centre are normalised by the sphere diameter. (The presence of oil in the plastic cylinder, included to reduce friction, leads to an optical distortion in the photograph; the measured ratio of sphere extension to sphere diameter (D=6.33mm) in x and y direction is about 0.98 and 1.11 respectively). **The error bars in this figure represent the uncertainty in the measurement of the sphere centres using ImageJ [23] The error is** ± 0.04 **of a sphere diameter in both the x and y directions.**

hard wall boundary conditions at the two ends of the chain. For any given axial compression the uniform zigzag structure can be characterised by a lateral displacement y which is the same for each sphere, and an angle θ. Between contacting

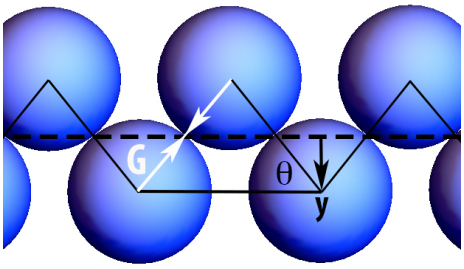

FIG. 2: The uniform *zigzag* structure is characterised by the same transverse displacement y and tilt angle θ for each sphere. There exists a compressive force G between all contacting spheres.

spheres there is a compressive force G (with no friction) - its horizontal component is $G_0 = G\cos\theta = \frac{1}{4}$ (in non-dimensional units, see [18]).

The uniform zigzag is an equilibrium solution for any compatible boundary conditions – but it is always unstable, except for very small N. If released from the condition of uniformity, it will undergo the localisation that is the subject of this paper, in order to reach a stable state. See Appendix A.

III. MODEL AND METHOD

We are concerned with a system of N hard spheres of unit diameter, confined between hard walls. The confining force at the walls (an important quantity in all later calculations) is G_0. In contact but uncompressed, the chain is of length $L = N$. For $G_0 > 0$ the compression will be represented by the parameter:

$$\Delta = N - L. \tag{1}$$

The total energy is given by,

$$E = \frac{1}{2}\sum_{n=1}^{N} {y_n}^2, \tag{2}$$

where y_n is the transverse displacement of the nth sphere from the central axis (for details of how the non-dimensional quantities are derived see [18]). Note that the model is confined to be *planar* because only planar structures are found in the regime that we explore, as may be confirmed by energy minimiation calculations not confined to two dimensions [19].

We search for equilibrium structures (stable or unstable): each sphere is in equilibrium under the action of contact forces and the confining force associated with the potential energy, given in eq. (2). We do so by the same shooting method adopted in [18]. This uses the following recursion relations to proceed from one wall to the other and searches for solutions consistent with both hard wall boundary conditions. The relations are:

$$\theta_{n+1} = \arctan\left(\frac{F_n}{G_0} - \tan\theta_n\right), \tag{3}$$

$$F_{n+1} = \sin\left[\arctan\left(\frac{F_n}{G_0} - \tan\theta_n\right)\right] - F_n. \tag{4}$$

Fig. 3 illustrates the significance of the parameters in eqs. (3) and (4): F_n is the force due to the harmonic potential on the nth sphere, θ_n is the tilt angle (i.e. the angle between the line connecting the centres of spheres $n-1$ and n and the central axis). Note that both F_n and θ_n are defined in such a way as to always to be *positive*. The direction in which they are measured alternates from one sphere to the next. All structures that are found are of a "zigzag" character, that is with alternating signs of displacement and angle (for a photograph of an example see Fig. 1), but

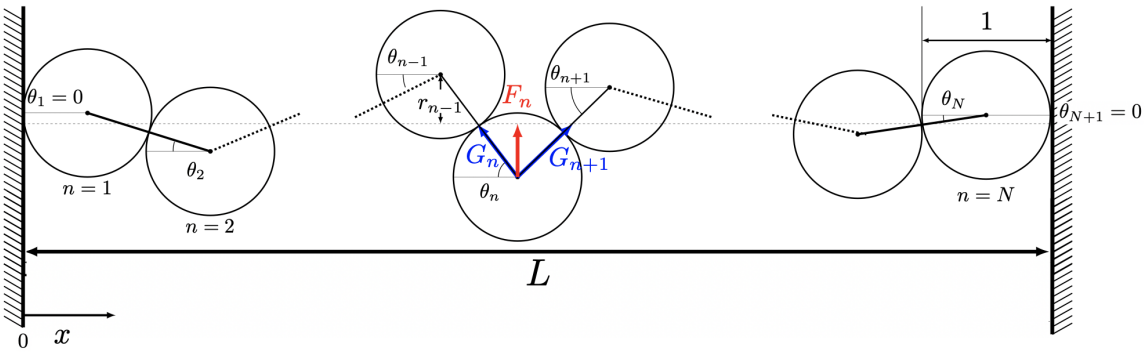

FIG. 3: Schematic for the analysis of a chain of hard spheres under compression, showing the role of the contact forces G_n, restoring forces F_n (equal to the transverse displacements y_n in the units used here), and contact angle θ_n. The horizontal coordinate of the centre of each sphere x_n, relates to the middle.

not uniform. G_0 is also positive and is the force exerted on each of the hard walls, normal to the wall.

The hard wall boundary condition for sphere $n = 1$ requires the first tilt angle θ_1 to be zero. For a chosen value of G_0, we proceed iteratively from an initial choice of F_1 to (F_{N+1}, θ_{N+1}). The angle θ_{N+1} corresponds to the contact of the Nth sphere with the wall, as illustrated in Fig 3. We search for values of F_1 (in general more than one) such that the angle θ_{N+1} is *zero*, satisfying the second hard-wall boundary condition. Note that the resulting solution is for given G_0, fixed during the iteration; compression Δ is not preset, but rather given as an output,

This search is performed by coarse graining the initial force F_1 over a range of $0 < F_1 \leq 0.5$ in steps of 10^{-4}. These values are then used as brackets in a bisection method. An exception to this is required when searching for a solution close to the termination points **(marking contact formation between next nearest-neighbour spheres)** for a given structure (as described in Section IV). This regime

was found to require smaller steps and enhanced accuracy.

Given any equilibrium structure determined in this way, we may compute the compression Δ, as

$$\Delta = N - \sum_{n=1}^{N} \cos\theta_n. \tag{5}$$

together with other quantities of interest. Some of these quantities are as follows.

The total energy E, Eqn 2, is an obvious choice. When we compare different buckled structures for the same compression, the difference of their energies will be relatively small. According we will adopt a definition of *relative energy*, given in Section IV.

Another useful output quantity is the value of the maximum displacement, here equal to F_{max}. We shall mainly use the tilt angle θ_n as a measure of local buckling.

The position of the peak **(maximum transverse displacement)** of a buckled chain is defined by the following weighted average of squared displacements,

$$x_p = \frac{\sum_n^N F_n^2 (x_n - L/2)}{\sum_n^N F_n^2}, \tag{6}$$

where is N is the number of spheres, x_n and y_n **(in the nondimensional units used here,** $y_n = F_n$**)** give the position of the nth sphere, and L is the chain length.

The width w of the peak is then defined as

$$w = 2\sqrt{\frac{\sum_n^N F_n^2 (x_n - x_p)^2}{\sum_n^N F_n^2}} \tag{7}$$

The shooting method described above is so efficient that very large amounts of data are easily generated in order to compile, for example, the comprehensive bifurcation diagrams presented below.

IV. EXAMPLES OF EQUILIBRIUM STRUCTURES AND BIFURCATION DIAGRAMS

At very low compression, equilibrium structures are *symmetric* about the midpoint between the two walls. The basic symmetry of the system requires that either this is the case, or the structures occur as equivalent pairs, related by reflection about the centre of the system. Fig 1 was an example of this. At higher compressions, asymmetric structures arise in pairs with positions $x_p = \pm x$.

In this section examples of equilibrium structures are shown and located on the relevant bifurcation diagrams.

There is no difficulty in applying the method to large values of N, of the order of 10^2 of more, but for present purposes of building up a clear picture of localisation properties, it is preferable to use small values. We have chosen $N = 5$, 6, 7, 8 as illustrations, in each case computing bifurcation diagrams and showing representative examples of equilibrium structures.

As already noted in [18], there is a distinct difference between systems of *odd* or *even* N as regards the stability/instability of the symmetric states. We shall discuss this for the examples that follow.

A. The case N=5

A representative sample of equilibrium structures for a system with $N = 5$ is shown in Fig. 4(a). Unstable structures are marked with an asterisk.

The bifurcation diagram Fig. 4b) shows the position of the buckling peak (as found by using eq (6)) against the compression Δ. Note that this is only half of the complete diagram, the other half being obtained by reflection in the horizontal axis. (See the above remark concerning symmetry.)

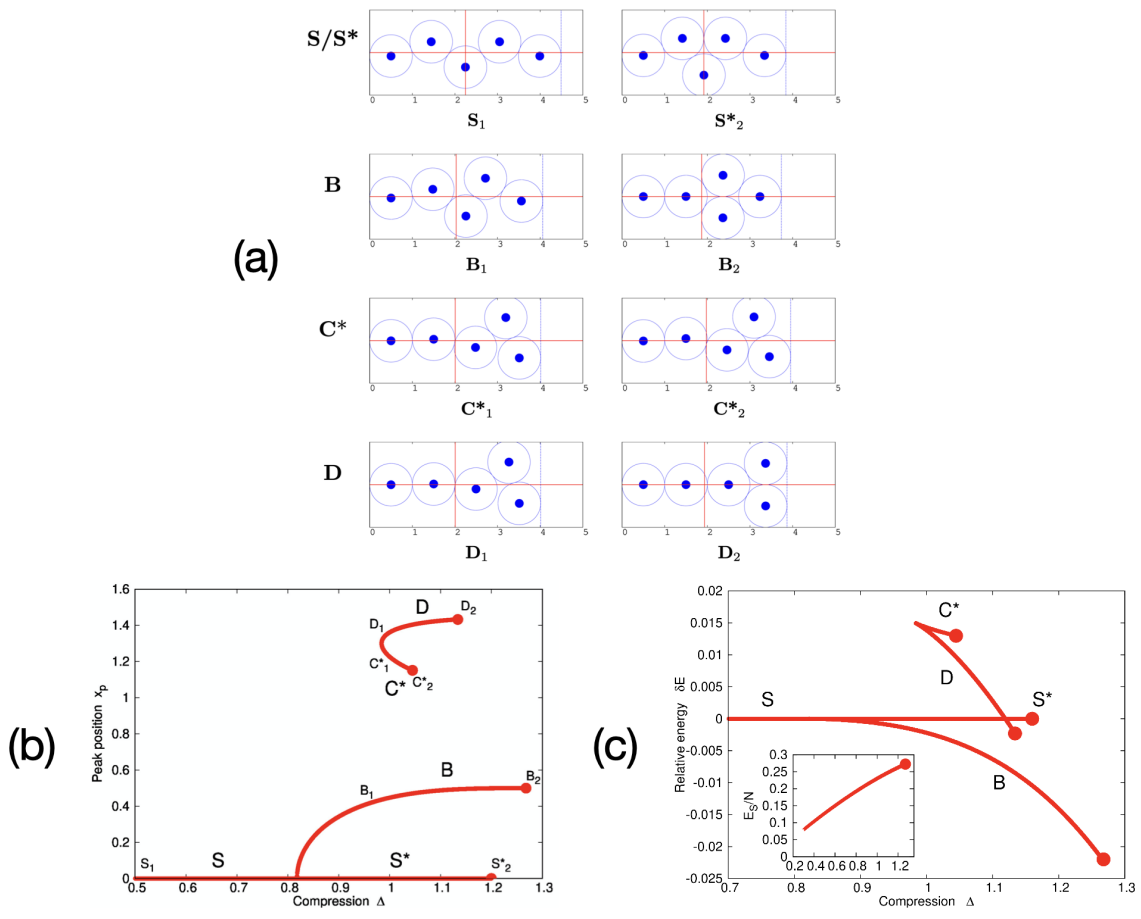

FIG. 4: Results for a chain of N=5 spheres. (a) The linear chain is bounded by two opposing hard walls, at $x = 0$ and $x = L$ (the second wall is indicated by a vertical dashed blue line). Blue dots indicate sphere centres. The horizontal red line marks $y = 0$ while the vertical red line shows the midpoint of the linear chain (i.e. $x = L/2$). The labels below each structure correspond to the location in the bifurcation diagrams at which that solution is to be found. (b) Bifurcation diagram for peak position and (c) for energy, relative to that of the symmetric structure. **Unstable solutions are marked with an asterisk.** The termination point of each branch is shown by a red dot. The inset in (c) shows the energy per sphere of the symmetric structure.

With the exception of the symmetric structure S (see below) the solutions found by the shooting method are labelled alphabetically in ascending order as indicated in Fig. 4b).

For low values of compression Δ the only solution is S, the symmetric structure, with buckling located at the mid-point of the chain. This solution is shown by the red line along the horizontal axis in Fig. 4b. An example of such a solution is shown in Fig. 4a and is labelled S_1, corresponding to point indicated in Fig. 4b.

With increasing compression the structure B emerges by a pitchfork bifurcation from the symmetric structure S. The buckling of the structure B is asymmetric, as shown by the image labelled B_1 in Fig. 4a.

At the onset of the pitchfork bifurcation, the symmetric arrangements becomes unstable and we label it S^* to indicate this. Continuing to compress the unstable symmetric structure further brings the two spheres adjacent to the central sphere ever closer until they eventually come into contact (S_2^* in Fig. 4a). At this point we terminate the solution.

We indicate all termination points by a red dot, as in Fig. 4b. While the present model can be used to follow the solution beyond such termination points (leading to overlap between next nearest-neighbour spheres), we do not show that unphysical result here.

With increasing compression a second pair of solutions emerges from an "out-of-the-blue" bifurcation, without any preceding structure. These are labelled C^* and D; they have their buckling peaks shifted even further towards the bounding walls. In the case of D, with increasing compression the structure eventually tends towards an arrangement with a pair of spheres against the bounding wall (labelled D_2, see Fig 4a).

Note that the structures as labelled in Fig. 4b alternate in *stability*. That is, if the symmetric structure is unstable then the next structure will be stable, and so

on. In our preliminary work (see [18]) the identification of stable/unstable structures was supported by energy minimisation calculations (which gave the stable modes). At this stage such confirmation is not necessary, as the alternating pattern of stable/unstable structures has been established.

Another quantity of interest is the relative energy of the structures. This we will define as the energy of a solution *relative to that of the symmetric structure* for the same value of compression Δ,

$$\delta E(\Delta) = E(\Delta) - E_{S/S^*}(\Delta), \tag{8}$$

where $E(\Delta)$ is the energy of the structure at a compression Δ and $E_{S^*}(\Delta)$ is the energy of the symmetric structure at the same compression. This is convenient, since the energy differences between all of these structures is very small. The total energy of the symmetric structure is indicated in an inset.

All of the qualitative features of these results apply to any case of *odd* N, except that the number of asymmetric structures increases with N.

Note that the bifurcation diagrams presented in [18] used a different (and more convenient) definition. This was the energy relative to that of the symmetric structure for the same compressive force G_0.

B. The case N=6

A representative sample of the equilibrium structures for $N = 6$ is shown in Fig. 5a, together with the accompanying bifurcation diagrams in Fig. 5b,c.

In the case of $N = 6$ (or any even N) the symmetric structure S is *always* a stable solution (as it is for all cases where N is even).

We again find that at low compressions the only equilibrium structure is the symmetric one. With increasing compression two new solutions appear from an out-

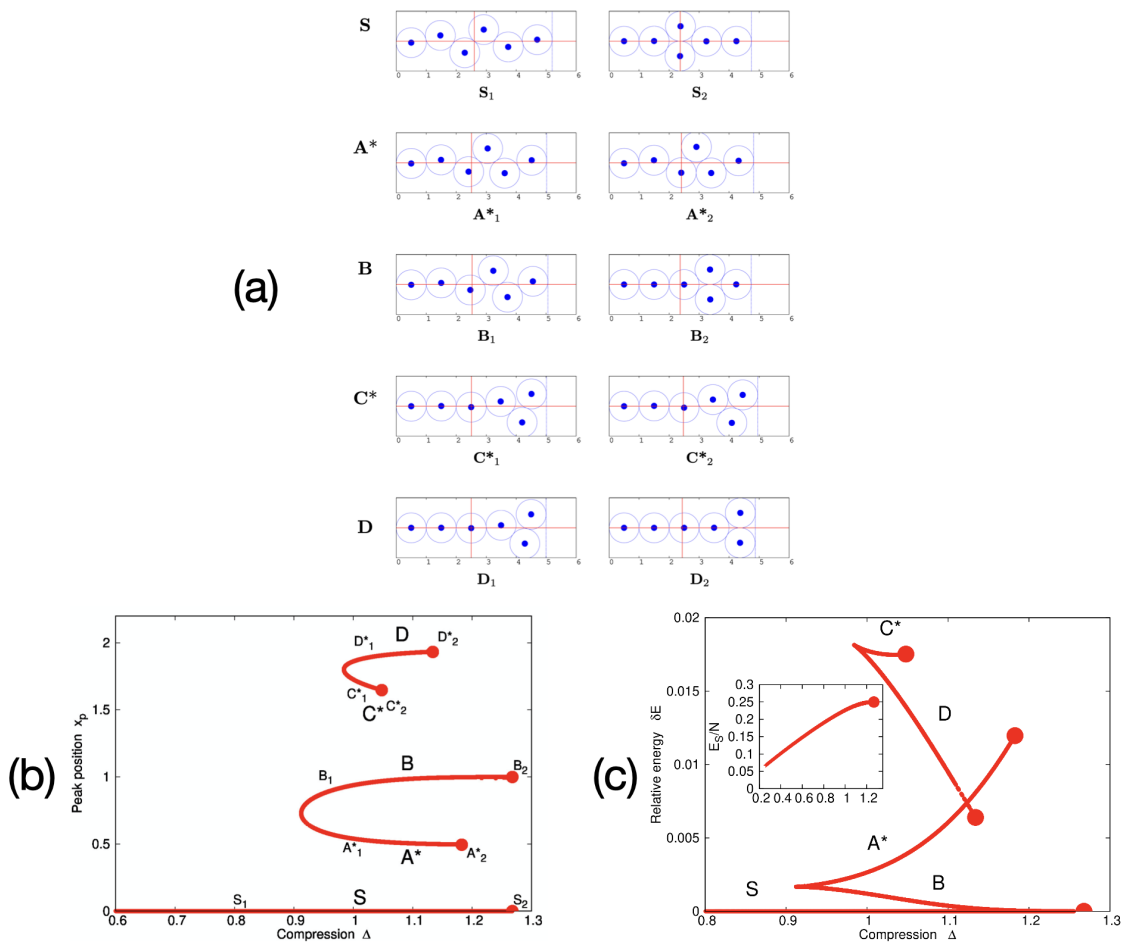

FIG. 5: Results for N=6 spheres: (a) Structures found using the shooting method. (b,c) bifurcation diagrams for peak position and energy, respectively. Again, unstable solutions are indicated with an asterisk. The notation is the same as for Fig. 4.

of-the-blue bifurcation as a stable/unstable pair, we label these states A^* and B; that is in order of the buckling peak position, as shown in Fig. 5a.

Finally, for larger values of compression a second out-of-the-blue bifurcation yields

another stable/unstable pair, which we label C^* and D.

C. The case N=7

A representative sample of the equilibrium structures for $N = 7$ is shown in Fig. 6, with the accompanying bifurcation diagrams in Figs. 6b,c. Since this is a case with an odd value of N the symmetric structure (S) is initially stable and then becomes unstable (S^*) at the pitchfork bifurcation.

D. The case N=8

A representative sample of the equilibrium structures for $N = 8$ is shown in Fig. 7 with the accompanying bifurcation diagrams in Figs. 7b,c. Since the value of N is even, the symmetric structure S is always stable.

E. Alternative Structures

These bifurcation diagrams are rich in detail, yet they are not to be taken to be complete. As has been noted by others [9–12], there are in principle further structures at higher energies. At the present stage these seem unlikely to have much significance for real physical systems. One may take *multiple* peaks as an example. For large enough Δ they are just simple combinations of single peaks, with some interaction between them. An example of such a structure (generated using the shooting method) with multiple peaks for $N = 10$ is shown in Fig. 8.

V. TERMINATION POINTS

At each termination point the equilibrium structure acquires at least one new contact. Illustrative examples were already included in Figs. 4, 5, 6 and 7.

For the symmetric structure, a chain with an even number of spheres takes the terminal form shown in Figs. 5 and 7, while in the case of a chain with an odd number of spheres it takes the form shown in Fig. 4 & Fig. 6

We may refer to that of Fig 5 (or Fig. 7), i.e. the arrangement labelled S_2 as a *doublet*. This simple equilibrium configuration can clearly be constructed anywhere in the chain, with the same compression $\Delta_{doublet} = 3 - \sqrt{3} \approx 1.2679$ and energy $E_{doublet} = 1/4$. The energy variation with Δ as this is approached is found to be quadratic close to the termination point.

$$E - E_{doublet} \sim (\Delta - \Delta_{doublet})^2 \tag{9}$$

Note also that for hard spheres the compression force G_0 is *zero* in the case of the doublet, so G_0 increases from 1/4 (the same value as for the uniform zig-zag) to a maximum and declines to zero, as compression Δ is increased from zero.

In general, asymmetric states appear to tend towards the doublet configuration, but they develop a single additional contact just before it is formed, and at this point we must stop, in the present work. In a real system a small further compression will bring the second extra contact into play and the perfect doublet structure will be found.

Asymmetric structures with a localized peak next to the wall may tend towards what we call a half doublet (e.g. structure F_2 in Fig. 7).

Once additional contacts have been formed, we enter a new regime, beyond the range of the present work. With further compression the doublet becomes the nucleus for the development of a new type of structure, which grows in extent until it takes

over the whole chain. In reality it is unstable with respect to a *twist*, so the structure becomes three-dimensional, if allowed to do so.

It should not be beyond the scope of the recursive method (suitably adapted) to pursue these higher structures, which require a different experimental technique from that shown here [18, 20]. We intend to undertake this continuation in the future. It should complement previous investigations [19]) on the full range of three-dimensional structures, which was based on energy minimisation.

VI. DEPENDENCE OF EQUILIBRIUM PROPERTIES ON COMPRESSION FOR A DISCRETE CHAIN

The localised buckling that is observed may be conveniently characterised by θ_{max}, the maximum value of θ. Its dependence on compression Δ is shown in Figs 9, for the case of $N = 8$. An initial increase of θ_{max} that is apparently of square-root form is followed by a broad linear regime, roughly speaking, before the terminal regime develops. Also shown are the variation of G_0 and F_{max} and the width w, defined in Section III.

While it is possible to discuss these variations within the discrete model, we have found it illuminating to develop a continuous description which provides relevant analytical results and approximations, particularly for small compression. In section VIII we also show experimental results of the variation of θ_{max} and width with compression.

VII. THE CONTINUOUS LIMIT

We have developed an approximate model in which θ, F, etc. are *continuous* functions of the variable u, which replaces n in the recursion relations for the discrete

case (Section III).

To do so we have reversed the familiar process by which *derivatives* are replaced by *finite differences* in numerical methods. This turns out to be a very fruitful approach, leading to analytic results, and helping to interpret the profiles of the discrete system for which we have presented results.

It has one major limitation: only the *symmetric* solution is found. Asymmetric states are a consequence of discreteness: see section IV.

Detailed analysis of the model leads us into some deep mathematics, particularly in relation to the theory of Jacobi elliptic functions. We will defer the exposition of this and other technical details to a later paper [21]: here we will concentrate on its results and their implications.

We shall investigate the continuous formulation for both finite and infinite systems.

A. Transition to the continuous model

The discrete model is described by the difference equations Eq (3) and Eq (4). To arrive at a single second-order equation for the angle $\theta(u)$, with $0 \leq u < \infty$ we proceed as follows. We define $\theta'(u) = \theta_{n+1} - \theta_n$, corresponding to a finite difference equation for $u = n + 1/2$. Similarly we set $\theta(u) = \frac{1}{2}(\theta_{n+1} + \theta_n)$. Using an equivalent procedure for the introduction of a displacement function $F(u)$ results in

$$F(u) = \frac{1}{2} \sin \left[\theta(u) + \frac{\theta'(u)}{2} \right], \tag{10}$$

where we have made use of Eqs (3) and (4).

Eq (4) can now be re-written in terms of the continuous functions $\theta(u)$, $F(u)$ and their first derivatives with respect to u. Further manipulation, involving differentiation of Eqn (10), then results in the following second order differential equation for

$\theta(u)$ in a continuum description,

$$2\sin\left(\frac{\theta'}{2}+\theta\right)-\left(\frac{\theta''}{2}+\theta'\right)\cos\left(\frac{\theta'}{2}+\theta\right)-8G_0\frac{\sin(2\theta)}{\cos 2\theta+\cos\theta'}=0. \qquad (11)$$

Eqn (11) looks unpromising, as it offers little hope of a closed-form solution. Indeed, for present purposes we will present numerical solutions using Mathematica.

In order to make sense of these results it is helpful to reduce the equation to something much simpler, with transparent properties and qualitatively similar solutions.

B. Reduction of the differential equation

For the following discussion we find it convenient to introduce a small quantity κ, $|\kappa|^2 \ll 1$, (called ϵ in our previous paper [18]), which may be real or imaginary, by defining

$$\kappa^2 = G_0^{-1} - 4. \qquad (12)$$

Eqn (11) may be reduced as follows, to arrive at a form which can be solved analytically. We first expand the sine and cosine functions to second order in θ and θ'. We then evaluate the magnitudes of the various terms involving products of θ, θ', θ'' and their powers in terms of the maximum value θ_{max} (peak) of a solution. The result is the non-linear differential equation which we refer to as *first reduced equation.*

First Reduced Equation:

$$\theta'' = \kappa^2\theta - 2\theta^3, \text{ for small } \kappa \text{ and } \theta \qquad (13)$$

which has proved to be useful. We will make only limited use of it here, and present a full analysis of its solutions, and further quantitative comparison with those of the full equation, in a further paper. Further reductions yield the

Second Reduced Equation:

$$\theta'' = \kappa^2 \theta, \text{ neglecting the } \theta^3 \text{ term} \tag{14}$$

and the

First Reduced Equation for $\kappa = 0$:

$$\theta'' = -2\theta^3. \tag{15}$$

C. Exact solutions

The value of the reduced (and hence approximate) equations lies in the availability of exact solutions. These will be described in detail in a subsequent paper: they have been used to validate the numerical treatment of the full equation, presented below.

The simplest example is that of the Second Reduced Equation (14), which is linear and has exponential solutions, given by

$$\theta(u) \sim \exp(\pm \kappa u). \tag{16}$$

These apply away from the peak, in the tails of the profile for the infinite case, as in Fig. 10.

The First Reduced Equation (13) has much more general applicability, and develops all the features of the solution of the full equation, for low compression. Its exact solution is given by

$$\theta(u) = \kappa \, sech(\kappa u), \tag{17}$$

The inflection points beyond which the exponential tails develop are at $u = (\ln \sqrt{2} \pm 1)/\kappa$.

The compression Δ may be evaluated using

$$\Delta = \int_0^\infty (1 - \cos\theta(u)) \, du. \tag{18}$$

Approximating $1-\cos\theta$ by $\frac{\theta^2}{2}$, we find that

$$\Delta \approx \kappa \approx \theta_{max} \text{ as } \kappa \to 0. \tag{19}$$

Further exact but less transparent solutions are provided by Jacobi functions which will be fully described in a subsequent publication [21].

D. Numerical solutions

We have used standard Mathematica routines to compute numerical solutions of the full equation (11) for both infinite and finite systems.

1. *Infinite system*

We model the infinite system by defining boundary conditions at a position well out in the exponential tail of the solution (here set at $u = 0$). For a given value of κ the conditions then are $\theta(0)/\theta_{max} = \theta(0)/\kappa \ll 1$, and $\theta'(0) = \kappa\theta(0)$, consistent with Eq (17). From the solution $\theta(u)$ we then obtain the corresponding value for compression Δ by numerically performing the integration of Eq (18). The force profile is computed from Eq (10).

As an example we show in Fig 10 tilt angle $\theta(u)$ and force profile $F(u)$ for $\kappa = 0.04$, resulting in a compression $\Delta = 0.03976$. (In this case we found setting $\theta(0) = 10^{-6}\kappa$ sufficiently small for independence of the profile from the value of $\theta(0)$.) For this compression the analytic solution of the First Reduced Equation, Eq (17), plotted as a dashed black line, provides an excellent approximation of the numerical solution $\theta(u)$ of the full equation. Deviations of the two solutions become apparent only for larger values of κ, and thus deformation, see the inset in Fig 10 which was produced for $\kappa = 0.35$, resulting in $\Delta = 0.328$.

We have repeated such calculations for a range of values of κ (and thus Δ). Fig 11 shows that in the limit of small compression, θ_{max} varies linearly with Δ, consistent with the analytic result of Eq (19) deduced from the solution of the First Reduced Equation, Eq (17).

2. *Finite system*

A finite chain of N spheres confined by hard walls at both end points is represented by $\theta(1) = 0$ and $\theta(N) = 0$. Only the first equation is directly implemented as a boundary condition in our numerical scheme. We have proceeded by setting $\theta'(1) = 2\arcsin(2F_1)$ (see Eq (10)) and increasing F_1 in a procedure similar to that used for the discrete case described in Section III. We thus search for a value of F_1 so that for a given value of κ the numerical solution of the full equation (Eq 11) results in $\theta(N) = 0$.

Fig 12 shows an example of the profiles $\theta(u)$ and $F(u)$ for $N = 10$ and $\kappa = 0.03$. The corresponding value of compression is computed from Eq (18), resulting in $\Delta = 0.164$.

Unlike in the infinite case (Eq (19)), for finite systems the value of $\kappa = 0$, i.e. $G_0 = 1/4$ (see Eq (12)), results in a *non-zero* compression Δ. To study the limit $\Delta \to 0$ we require values of $G_0 > 1/4$, ie $\kappa^2 < 0$, corresponding to imaginary values of κ (i.e. $\kappa = i\mu$). Solutions at such low compression have a different qualitative form. Whereas the finite tails may be approximated by sinh functions at the boundaries for positive κ (instead of exponentials that we noted in the infinite case), imaginary κ implies a profile proportional to $\cos(\mu u)$ as $\Delta \to 0$ (c.f. Second Reduced Equation, Eqn (14)). In that limit we obtain $\frac{\pi}{\mu} = N$, to fit both boundary conditions.

Fig 13 shows the variation of κ^2 with Δ, again for the case $N = 10$, consistent with the above description. While for the infinite system, κ^2 remains positive for

all values of Δ, there is a cross-over to negative values in the case of finite N. Its value may be estimated using the First Reduced Equation for $\kappa = 0$, Eq (15), as $\Delta_c = \pi/(2N)$ [21].

Fig 14 shows that the two regimes i.e. $\kappa^2 \lesseqgtr 0$ (or $G_0 \lesseqgtr 1/4$), are significant for the variation of θ_{max} (and other quantities) on Δ. Whereas for $\kappa^2 > 0$, where the solution approaches that of an infinite system, a roughly *linear* dependence is found (see Fig 11), there is roughly a square-root form for $\kappa^2 < 0$ and this may be shown in the exact asymptote form.

The same distinction was seen in the earlier computation for the discrete chain ([18] and Fig 9), and could be explained directly, but the continuous model provides a relatively transparent interpretation.

VIII. EXPERIMENTS

In the previous sections we have presented a number of numerical results which invite comparison with experiments. In earlier work our interest lay mainly in the many three-dimensional structures found under higher compression and we used a lathe to create a harmonic confining potential [18, 20]. Recently we have demonstrated a much simpler experimental set-up that is sufficient for the regime considered in this paper. Hard spheres (e.g. ball bearings) placed in a horizontal cylindrical tube, exhibit all of the localisation properties described here (see [22] for full details). Provided that the diameter of the tube is much greater than that of the spheres, the system is approximately planar. Gravity gives rise to the quadratic potential included in the model. We have used such a system to provide illustrations of the theoretical results of this paper; one was already shown in Fig 1 for compression $\Delta = 1.04$.

All of these experiments were carried out using eight steel spheres (ball bearings)

with diameter $D = 6.33$ mm, confined in a transparent cylindrical tube with inner diameter 20.05 mm. The tube is closed with stoppers at each end, with one stopper being moveable, so that the tube volume can be smoothly adjusted in the course of an experimental run. In order to decrease friction between the spheres we immersed them in vegetable oil. A small hole in the upper half of the tube allows for the escape of air, as the stopper is pushed inwards. A spirit level was used to facilitate horizontal alignment of the tube. Compression Δ is given by $\Delta = N - L/D$, where L is the chain-length; all our experiments were for $N = 8$ spheres.

Figure 15(a) shows a sequence of photographs of a chain of eight spheres for increasing values of compression. Buckling is seen to occur around the centre of the chain (symmetric peak), c.f. structure S in our simulations shown in Fig 7.

From image analysis (using ImageJ [23]) we are able to measure positions and hence angles of the structure. The angle profiles θ_n, shown in Figure 15(b), are found to be in good agreement with simulations, of the kind described in Sections III and IV. The increase of the maximum tilt angle as a function of compression, and the corresponding decrease of the width of the angle profile, features also in our discrete simulations, see figure 9(a).

IX. CONCLUSION

We have completed an analysis and interpretation of some of the key properties of the linear chain of hard spheres under confinement and compression. Understanding of the system is fairly complete and it can be said to stand as a prototype for various physical systems of interest. We have deferred to a later publication the mathematical developments, involving Jacobi functions, that are mentioned in Section VII.

At the same time, it is itself amenable to experiment, of which we have shown a simple example. One further experiment we intend to conduct is the investigation

of the Peierls-Nabarro potential. This is the apparent potential, given as a function of position, experienced by the localised peak of buckling when it is moved by an added force. It is a continuous potential, including the values for energy for stable and unstable solutions (e.g. Fig 4c) as minima and maxima of a continuous curve. It may also be determined by computation in an extension of the methods presented here.

Appendix A: What accounts for the phenomenon localisation of buckling?

We have seen that the localisation is a general feature of the buckling of the linear chain under confinement. One may rationalise this phenomenon by the following argument, starting from the uniform (non-localised) zigzag structure of Section II .

Consider a long finite zigzag structure of N spheres under fixed compression. This is to be compared with a second configuration, in which only a smaller section, consisting of only M spheres, has a uniform zigzag structure (necessarily of greater amplitude, in order to maintain the same value of compression), while the remainder consists of the straight chain (zero displacement). It is easy to show that the energy of this localised configuration is smaller than that of the original, if we ignore boundary contributions where the two structures meet.

This implies a reduction of energy upon reducing M, until boundary effects intervene to limit it, in a crude form of localisation.

ACKNOWLEDGMENTS

SH was supported by Science Foundation Ireland (SFI) grant 13/IA/1926 and the European Space Agency. AI acknowledges funding from the TCD Provost's PhD Project Awards. AM acknowledges the support of the Supercomputing Wales

project, which is part-funded by the European Regional Development Fund (ERDF) via Welsh Government.

---

[1] Y. Zhang, M. J. Godfrey, and M. A. Moore, arXiv: Soft Condensed Matter (2020).

[2] S. S. Ashwin, M. Zaeifi Yamchi, and R. K. Bowles, Phys. Rev. Lett. **110**, 145701 (2013).

[3] S. Varga, G. Balló, and P. Gurin, Journal of Statistical Mechanics: Theory and Experiment **2011**, P11006 (2011).

[4] C. Moore, D. Liu, B. Ballnus, M. Karbach, and G. Müller, Journal of Statistical Mechanics: Theory and Experiment **2014**, P04008 (2014).

[5] A. Ramirez-Pastor, P. Centres, E. Vogel, and J. Valdés, Physical Review E **99** (2019).

[6] M. Mielenz, J. Brox, S. Kahra, G. Leschhorn, M. Albert, T. Schätz, H. Landa, and B. Reznik, Physical Review Letters **110**, 133004 (2013).

[7] K. Pyka, J. Keller, H. L. Partner, R. Nigmatullin, T. Burgermeister, D. M. Meier, K. Kuhlmann, A. Retzker, M. B. Plenio, W. H. Zurek, A. del Campo, and T. E. Mehlstäubler, Nature Communications **4**, 1 (2013).

[8] R. C. Thompson, Contemporary Physics **56**, 63 (2015).

[9] H. L. Partner, R. Nigmatullin, T. Burgermeister, J. Keller, K. Pyka, M. B. Plenio, A. Retzker, W. H. Zurek, A. del Campo, and T. E. Mehlstäubler, Physica B: Condensed Matter **460**, 114 (2015).

[10] R. Nigmatullin, A. del Campo, G. De Chiara, G. Morigi, M. B. Plenio, and A. Retzker, Physical Review B **93**, 014106 (2016).

[11] L. Yan, W. Wan, L. Chen, F. Zhou, S. Gong, X. Tong, and M. Feng, Scientific Reports **6**, 21547 (2016).

[12] H. Landa, B. Reznik, J. Brox, M. Mielenz, and T. Schätz, New Journal of Physics **15**,

093003 (2013).

[13] A. Melzer, Physical Review E **73**, 056404 (2006).

[14] T. Beatus, T. Tlusty, and R. Bar-Ziv, Nature Physics **2**, 743 (2006).

[15] A. V. Straube, R. P. A. Dullens, L. Schimansky-Geier, and A. A. Louis, The Journal of Chemical Physics **139**, 134908 (2013).

[16] L. Helseth, T. Johansen, and T. Fischer, Physical Review E **71**, 062402 (2005).

[17] D. Vella, E. du Pontavice, C. L. Hall, and A. Goriely, Proceedings of the Royal Society A: Mathematical, Physical and Engineering Sciences **470**, 20130609 (2014).

[18] J. Winkelmann, A. Mughal, D. Weaire, and S. Hutzler, EPL (Europhysics Letters) **127**, 44002 (2019).

[19] J. Winkelmann, A. Mughal, D. B. Williams, D. Weaire, and S. Hutzler, Phys. Rev. E **99**, 020602 (2019).

[20] T. Lee, K. Gizynski, and B. A. Grzybowski, Advanced Materials **29**, 1704274 (2017).

[21] D. Weaire, A. Mughal, and S. Hutzler, in preparation (2020).

[22] D. Weaire, A. Irannezhad, A. Mughal, and S. Hutzler, American Journal of Physics **88**, 347 (2020).

[23] M. D. Abràmoff, P. J. Magalhães, and S. J. Ram, Biophotonics International **11**, 36 (2004).

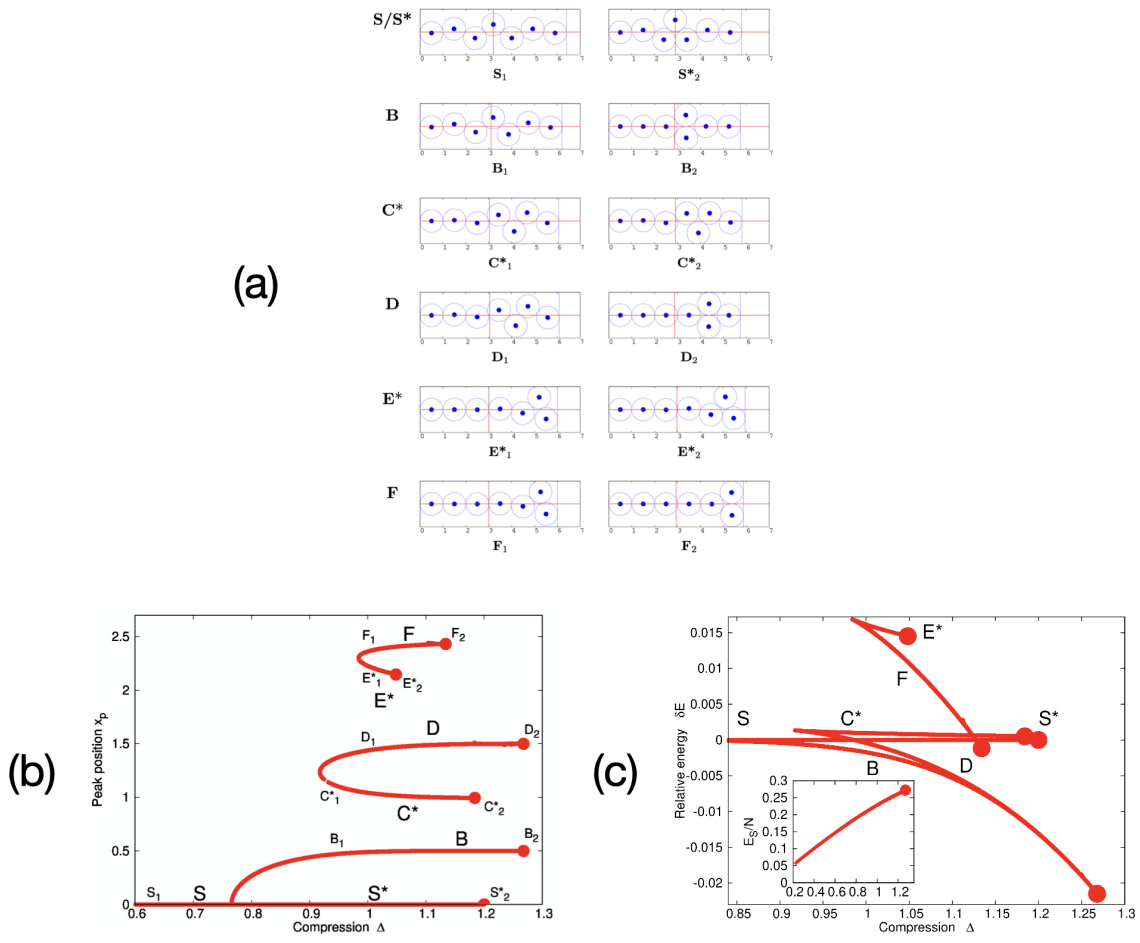

FIG. 6: Results for N=7 spheres: (a) Structures found using the shooting method. (b,c) Bifurcation diagrams. Notation details are the same as for Fig. 4. **The disconnected regions apparent in the diagrams for C_1^* and for (b) and the branch of E^* are an artefact of the simulation and in principle can be removed by using a smaller step size**

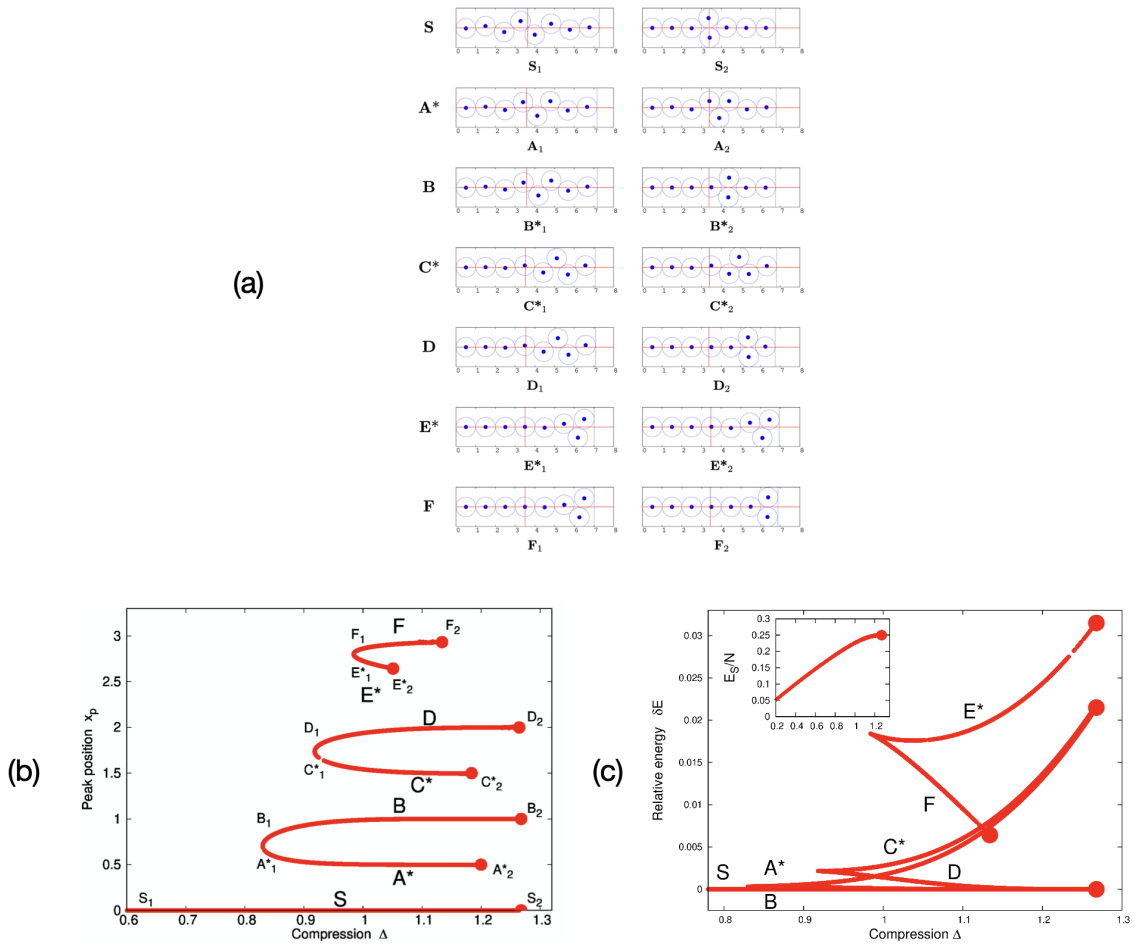

FIG. 7: Results for N=8 spheres: (a) Structures found using the shooting method. (b,c) Bifurcation diagrams, details of the notation are the same as for Fig. 4.

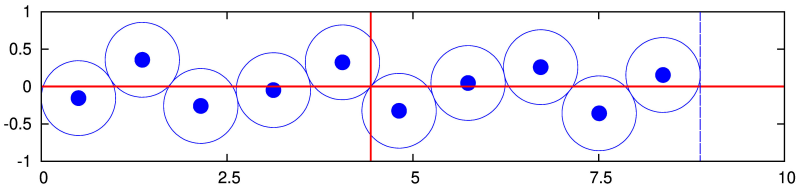

FIG. 8: A linear chain for $N = 10$ displaying multiple peaks of transverse displacement.

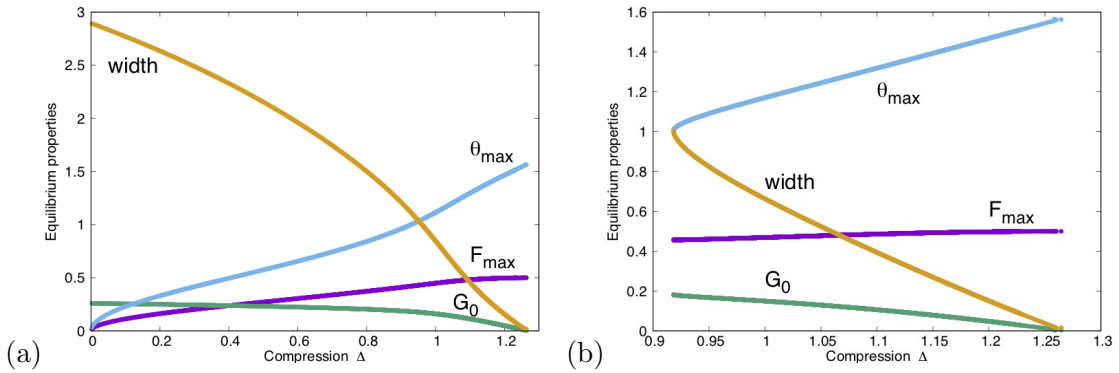

FIG. 9: Variation of G_0, θ_{max}, F_{max} and width w as functions of compression for a chain of $N = 8$ spheres for (a) symmetric and (b) asymmetric case (structure D).

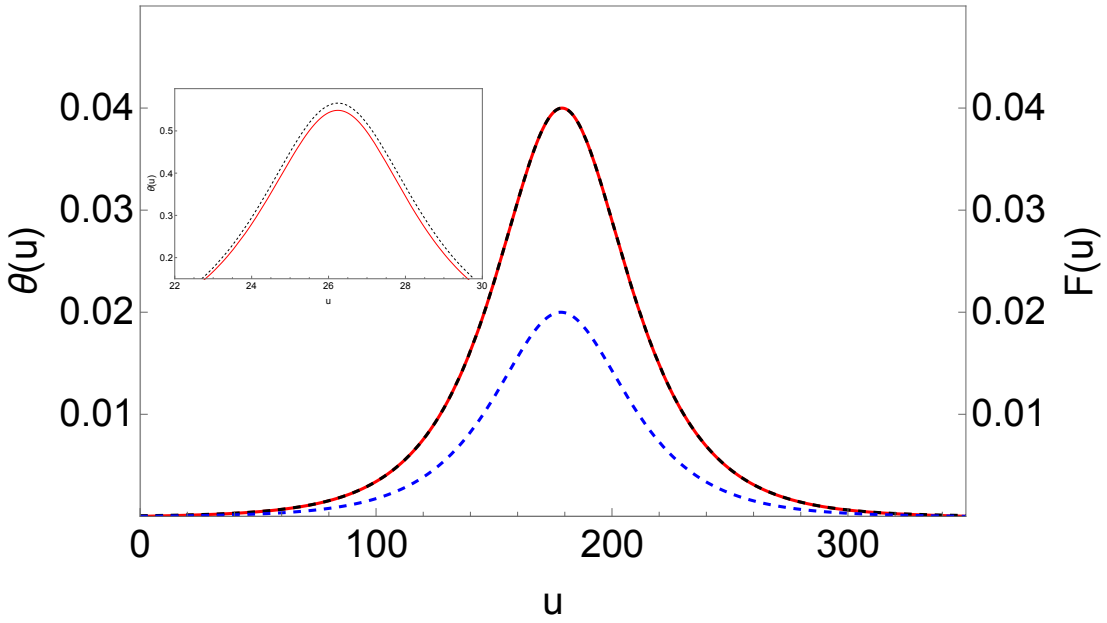

FIG. 10: Profiles of tilt angle $\theta(u)$ (red solid line) and corresponding forces (displacements), $F(u)$ (blue dashed line), as obtained from a numerical solutions of Eqn (11) for an infinite system with $\kappa = 0.04$, resulting in a value for compression $\Delta = 0.0398$. The analytical solution of the First Reduced Equation, Eqn (17) (dashed black line), provides an excellent approximation for $\theta(u)$. Only for higher values of κ are differences around the peak noticeable, as is seen in the inset for $\kappa = 0.35$, corresponding to compression $\Delta = 0.328$. (Note that the analytical solutions are shifted along the u-axis so that their peak positions match those of the numerical solutions.)

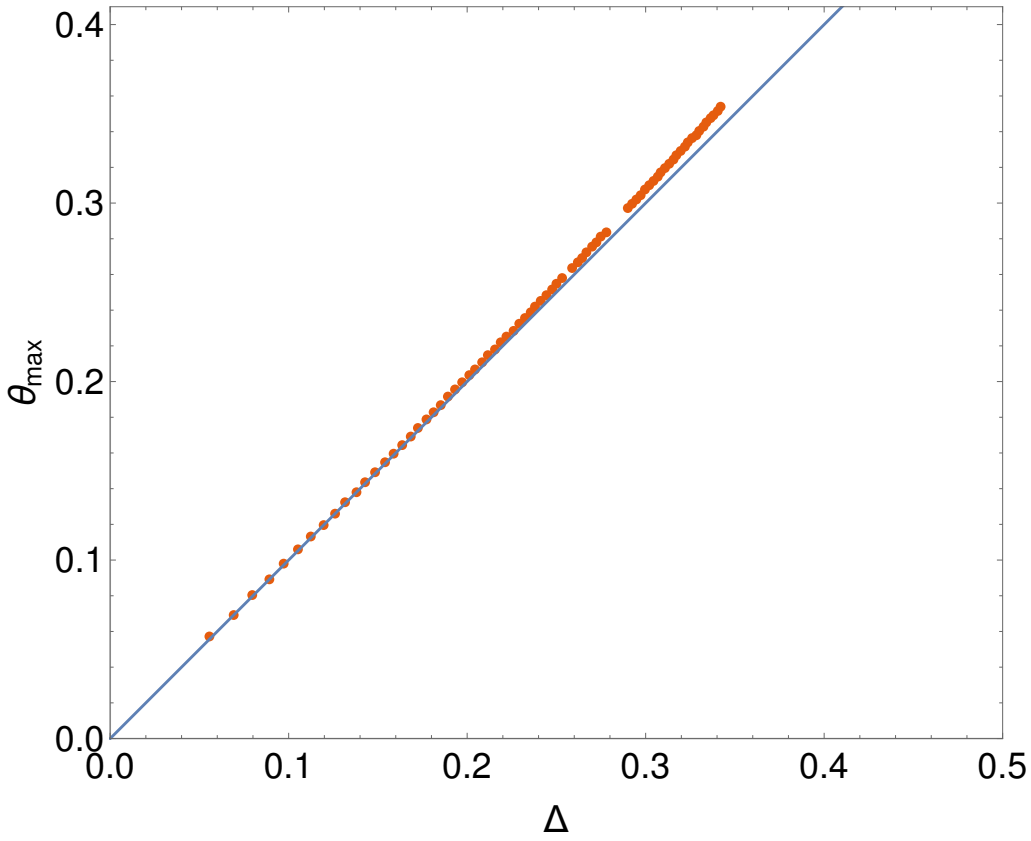

FIG. 11: Variation of θ_{max} with compression Δ for an infinite system. Data points are from numerial solutions of the full differential equation, eqn.(11). The line of slope unity represents the analytical result obtained for the reduced equation for low compressions, Eqn (19).

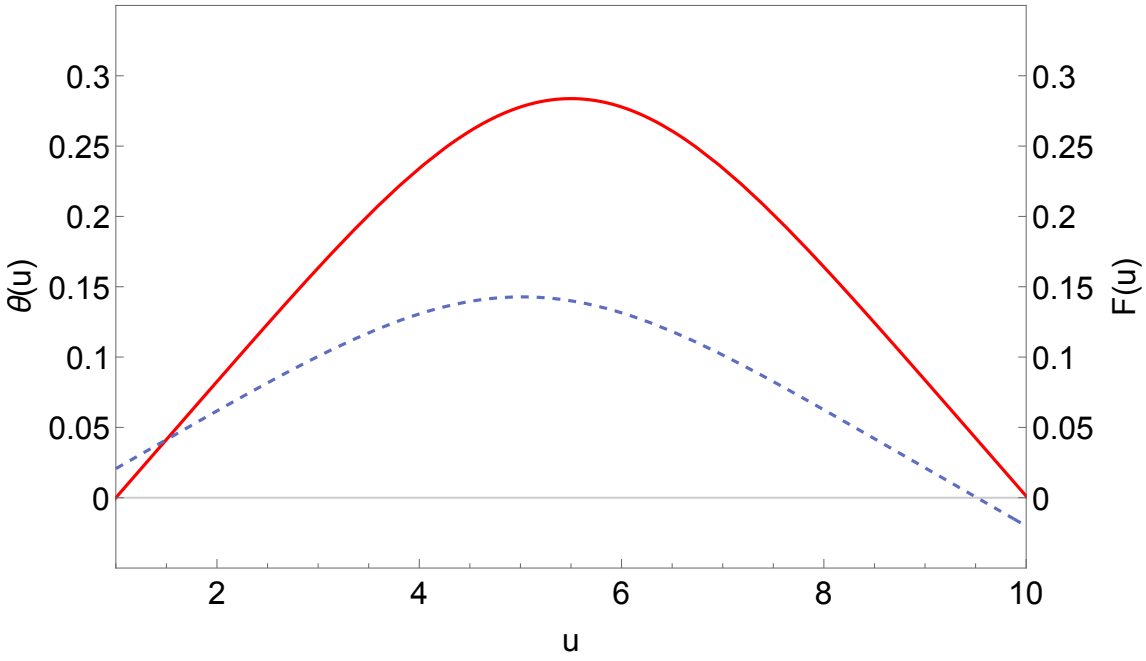

FIG. 12: Profile $\theta(u)$ (red solid line) for the case $N = 10$ and $\kappa = 0.03$. This results in a compression $\Delta = 0.164$. The profile takes on a roughly sinusoidal form, rather than the form of sech(u) seen in the infinite case. The force profile $F(u)$, obtained from Eq (10), is shown as a blue dashed line.Its maximum is shifted relative to the maximum of θ, as $\theta'(u)$ is no longer small throughout the solution, as per equation Eq (10).

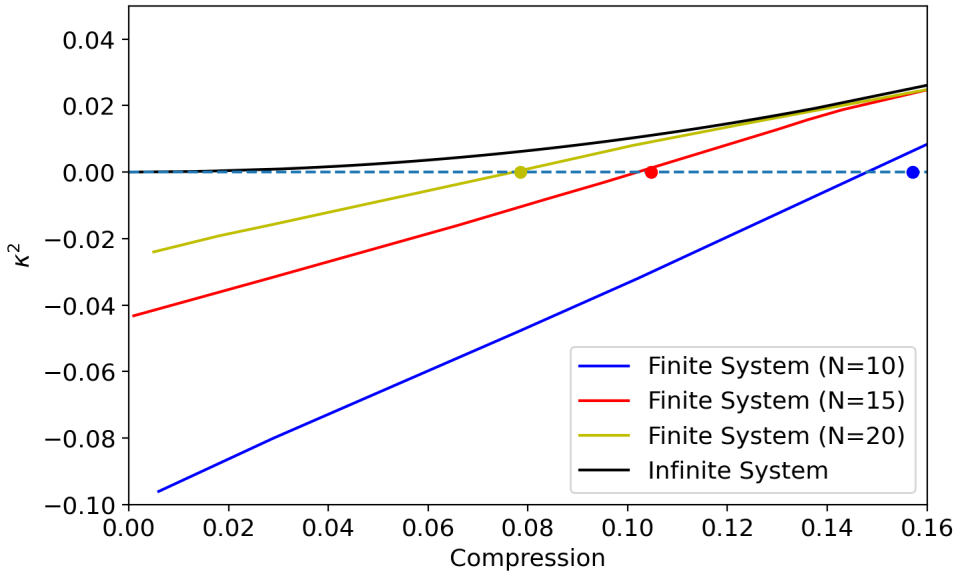

FIG. 13: The variation of κ^2 as a function of compression shows a qualitative difference for the cases of finite or infinite chain. Finite systems (here represented by numerical solutions of the full differential equation, Eq (11) for N= 10, 15, 20) show a change in the sign of κ^2. This is accompanied by a change of the functional form of the profiles for $\theta(u)$ and $F(u)$. For the infinite system (Section VII D 1) κ remains positive for all values of compression. The points marked on the $\kappa^2 = 0$ line represent predictions from analytic results of the reduced equation (for details see [21]).

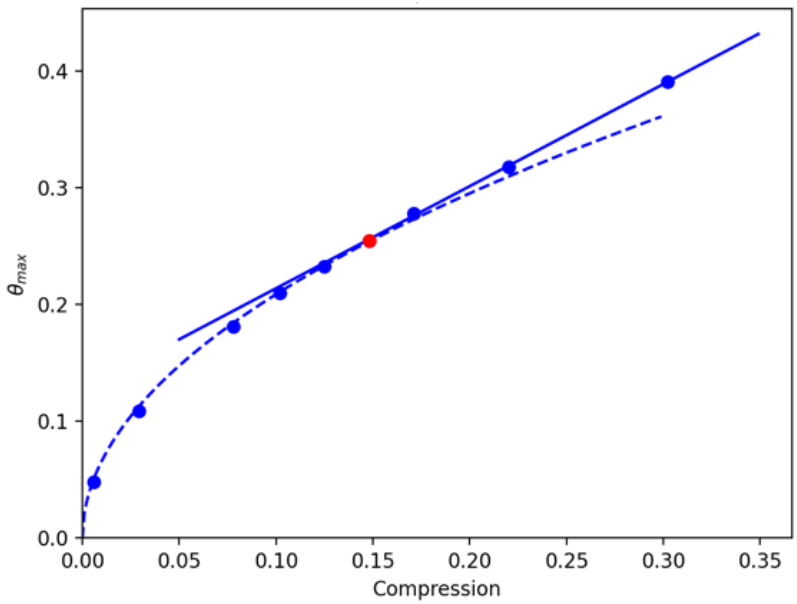

FIG. 14: Variation of θ_{max} as a function of compression Δ for $N = 10$ as obtained from numerical solutions of the continuous model, Eq 11. While for low compression $\theta_{max} \propto \Delta^{1/2}$ (dashed line), for higher compression the variation is linear (solid line). The point marked in red corresponds to the critical value of compression $\Delta_c = \pi/20 \simeq 0.156$, at $\kappa = 0$ ($G_0 = 1/4$), as computed from the First Reduced Equation for $\kappa = 0$, Eq (15)[21].

(a)

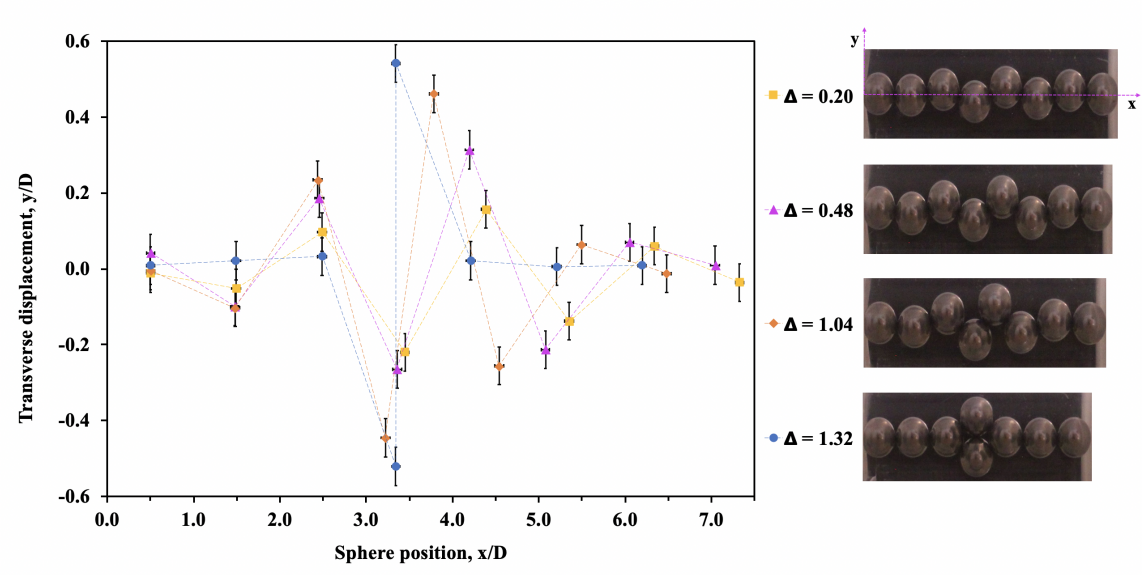

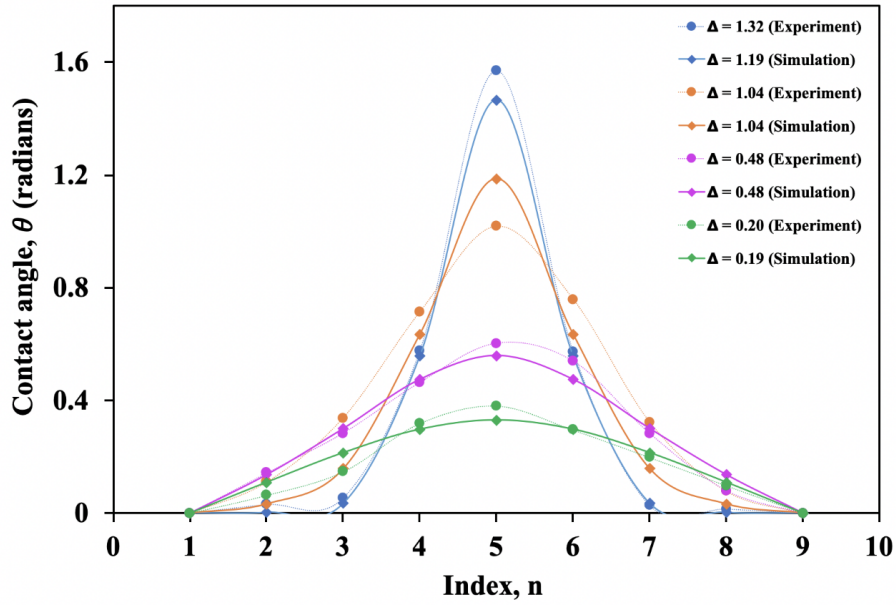

(b)

FIG. 15: Experimental data for a chain of N=8 hard spheres for four different values of compression Δ. (a) Transverse displacement profiles. At compression $\Delta = 1.32$ we observe a doublet structure. (b) Profiles of contact angles θ_i for several values of compression. The experimental data is roughly matched by our numerical results.